Damage Detection of Composite Laminate Structures Using VMD of FRF Contaminated by High Percentage of Noise

Sahar Hassani[a], Mohsen Mousavi[*b], Amir H. Gandomi [*b]

[a] *Faculty of Engineering, Department of Civil Engineering, Ferdowsi University of Mashhad, Mashhad, Iran*
[b] *Faculty of Engineering and IT, University of Technology Sydney, Ultimo, NSW 2007, Australia*

Abstract

A novel highly robust-to-noise and closely-situated eigenvalues damage detection method is proposed. The proposed method employs the Variational Mode Decomposition (VMD) to construct a new set of input signals obtained from the rows of the condensed Frequency Response Function (CFRF) to be used in a sensitivity-based model updating problem. Each row of the FRF matrix is replaced by its Unwrapped Instantaneous Hilbert Phase (UIHP). However, since the signal corresponding to the rows of the CFRF might not exhibit the mono-component property, and thus the UIHP will not be well-defined, VMD is used to obtain a set of constructive mono-component modes for each row, whereby the sum of UIHPs (SUIHP) for that row is obtained. The obtained SUIHPs for all rows of the CFRF are stacked up to obtain a new matrix to be fed into the optimisation problem. The proposed method is tested on a composite laminate plate with different configurations, as an example of structures with closely-situated eigenvalues. The results of the application of highly noisy measurement data for damage detection as well as comparison with two other methods demonstrate the superiority of the proposed method in damage detection of structures with closely-situated eigenvalues using highly noisy input data.

Keywords: Damage identification, Variational mode decomposition, Hilbert transformation, Frequency response function, Composite laminate structures, closely-situated eigenvalues

Email addresses: mohsen.mousavi@uts.edu.au (Mohsen Mousavi*), gandomi@uts.edu.au (Amir H. Gandomi *)

1. Introduction

Composite materials are being widely used in different fields of engineering such as civil infrastructures, automotive, and aerospace industry due to their numerous advantages over some traditional alternatives in different industries [1]. However, they are known to be susceptible to different damage mechanisms, arising either during the manufacturing process or load-bearing experiences in the field, such as fiber failure, matrix cracking, buckling, and delamination [2, 3, 4, 5, 6]. The performance of the structure under damage scenarios as such can be considerably compromised, where, if not identified and fixed, a total destruction of the structure is inevitable.

Hence, developing new damage identification methods helps with several factors such as increasing the safety, efficiency and durability of such structures plus reducing the costs associated with their maintenance [7]. Model updating methods seek to update structural parameters through minimising an error function which is typically constructed based on the difference between the response of the intact and damaged structures [8]. As such, a Finite Element Model (FEM) of the structure is usually assumed to be available, whereby any changes in the structural response due to damage can be accounted for through introducing degradation to the stiffness and mass matrices of the FEM [9]. Model updating methods are iterative algorithms, meaning that they are set up to update the unknowns in the FEM through iterations. To this end, various structural static and/or dynamic responses such as FRFs [10], modal information [11, 12], time histories [13], and strain responses [14] have been used by researchers.

There are generally two main groups of the model-updating techniques. These are: (1) optimisation-based, and (2) sensitivity-based algorithms [15, 16]. The former seeks to optimise an objective function constructed from some input data obtained from both real structure and its available FEM. Advanced optimisation algorithms are typically employed to solve the optimisation problem of this sort of problems [12]. The latter methods, however, are based on the sensitivity analysis of the structural vibration data obtained from the FEM with respect to the unknowns in order to reduce its distance from those obtained from the real structure. As such, sensitivity-based model updating methods seek to minimise a penalty function of errors obtained from the difference between the measured and simulated structural responses to some certain loads [17]. Sensitivity-based methods have been of great interest to researchers, because they can be used to robustly update the FEM of the structure which can be further used to reproduce measured responses. The main disadvantage of these algorithms is that they usually modify the most sensitive element instead of the one in error. To address this issue, it was recommended that the errors be first localised, and then changes be allowed to occur in the corresponding elements [17]. Model-updating techniques solve the problem of the damage detection either in one stage, as is the case for the sensitivity-based methods [18, 19, 16], or in two stages in some optimisation-based model-updating methods [12, 20]. The two-stage optimisation-based model-updating methods are also known as “hybrid” methods [9]. Some state-of-the-art two-stage damage detection methods can be found in [12, 1, 21].

The type of the input data plays an important role in the success of model-updating algorithms. Modal information such as natural frequency and mode shapes have been widely used in model-updating problems. However, they can impose some limitations on the process of updating damage indices. For instance, the modal data can only represent the effect of damage on resonance modes. This can be troublesome, especially in the case of structures with closely-situated eigenvalues where the information is lost due to some repetitive modes. The presence of the closely-situated eigenvalues can bring about a significant uncertainty in the structural modal responses which can further reduce the precision of damage detection algorithms. The main reason is that the modal responses of such structures are highly sensitive to small variations of the mass or stiffness matrices. Therefore, using modal data for damage detection of such structures is not a good choice [22]. Frequency Response Functions (FRFs) can be alternatively used to deal with the problem of closely-situated resonances. Moreover, FRF data obtained from vibration tests can better characterise the structural dynamic behavior. In addition, FRFs do not require any pairing or matching like mode shapes. Hence, some methods have been developed based on the application of FRFs in optimisation algorithms to solve the problem of the structural damage detection [23, 24, 25].

Although using FRFs for damage detection of structures with closely-situated eigenvalues is promising, they are still susceptible to measurement noise. One way to deal with this problem is to apply advanced signal processing techniques, whereby a new robust-to-noise signal can be constructed from the decomposed modes of the original input signals [26]. To this end, time-frequency signal processing algorithms can be employed to identify a set of Intrinsic Mode Functions (IMFs) out of the original input signal. The IMFs obtained from the decomposition process posses two following properties: (1) each IMF is mono-component and thus involves one mode of oscillation of the original signal only. As such, its frequency content is limited within a narrow-band around a center frequency, and (2) the sum of the IMFs can construct the original signal[1]. The first property of such IMFs makes it possible to define the instantaneous frequency, phase, and amplitude for them. As such, some instantaneous properties of the original signal, such as phase, can be obtained through summation of such properties taken over all of its IMFs. Some of the famous signal decomposition algorithms have been used for structural damage detection, some examples of which include: using wavelet transformation [27, 28], empirical mode decomposition (EMD) [29], ensemble empirical mode decomposition (EEMD) [30], and Variational mode decomposition (VMD) [31].

These methods can be also used for denoising input signals in damage detection algorithms, especially as for damage detection of composite structures with closely-situated eigenvalues. In this paper, a novel sensitivity-based model-updating method is proposed for damage detection of composite laminate structures with closely-situated eigenvalues. Therefore, the proposed method solves the problem of the damage detection in one stage. The constructed objective function uses the sum of the Unwrapped Instantaneous Hilbert Phase (SUIHP) of the rows of the decomposed FRF using the Variational Mode Decomposition (VMD) algorithm [32].

It is known that measuring the rotational DOFs can be challenging. Therefore, in this paper, the condensed FRF (CFRF) matrix is used to deal with the lack of information stemming from unmeasured rotational DOFs. As such, it is shown that using the SUIHP of CFRF can increase the accuracy of the damage detection results at the presence of high percentage of measurement noise. The proposed method is employed to solve the problem of damage detection in two models of laminated composites, the results of which are compared against two other methods proposed in [20, 12]. Three performance criteria are employed to evaluate the performance of the proposed method. These are: relative error (RE), mean sizing error (MSE), and the closeness index (CI). The results demonstrate the effectiveness of using the proposed SUIHP as opposed to the the CFRF for damage detection of composite structures with closely-situated eigenvalues.

2. The proposed SUIHP of the CFRF using VMD

In this section, the theoretical backgrounds of the proposed SUIHP constructed based on CFRF are presented. Each row of the proposed SUIHP is obtained from the sum of the Unwrapped Instantaneous Hilbert Phase (SUIHP) of the IMFs pertaining to the decomposition of that row using the Variational Mode Decomposition (VMD) algorithm (Figure 1). The VMD is employed to obtain a set of narrow-band oscillation modes (IMFs) for each row of the measured CFRF. As such, the UIHP of each IMF, corresponding to the decomposition of the row, is well-defined, and can be obtained from Gabor's analytical signal discussed in the sections to follow. The sum of all UIHP signals (SUIHP) corresponding to all IMFs of a row is replaced by the corresponding row in the CFRF matrix. Repeating the above procedure for all rows of

[1] In some cases, such as Variational Mode Decomposition, the perfect reconstruction can depend on the settings.

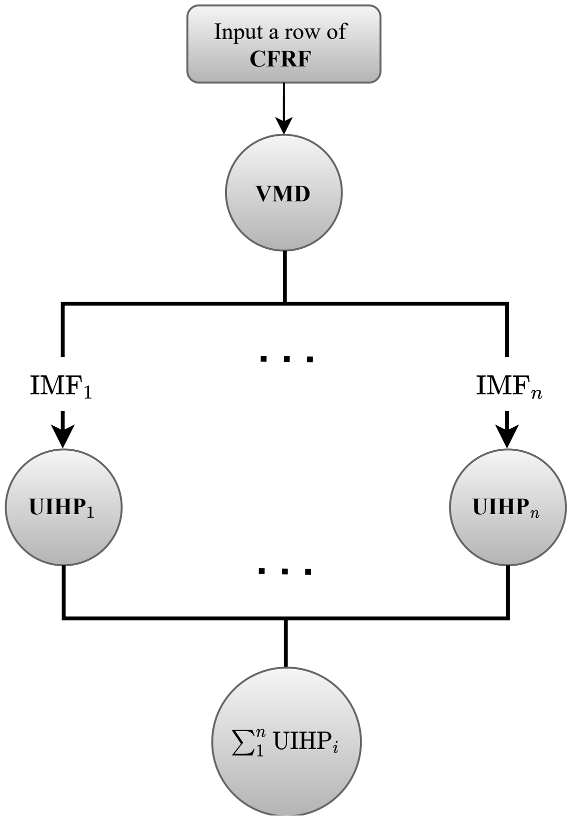

Figure 1: The flowchart of the proposed SUIHP of CFRF.

CFRF leads to a new matrix construction that can be further used for damage detection in a sensitivity-based model-updating problem. Note that in this paper SUIHP can refer to a row of the obtained matrix or the entire matrix depending on the context.

The details of the VMD algorithm and the calculation of UIHP for each extracted IMF is discussed in the following sections. However, first a brief definition of the CFRF is presented in the following section.

2.1. Definition of CFRF

A partitioned form of the stiffness, mass, and damping matrices of a structure is written as follows:

$$K = \begin{bmatrix} K_{m\times m} & K_{m\times s} \\ K_{s\times m} & K_{s\times s} \end{bmatrix} \tag{1}$$

$$M = \begin{bmatrix} M_{m\times m} & M_{m\times s} \\ M_{s\times m} & M_{s\times s} \end{bmatrix} \tag{2}$$

$$C = \begin{bmatrix} C_{m\times m} & C_{m\times s} \\ C_{s\times m} & C_{s\times s} \end{bmatrix} \tag{3}$$

where m and s denote the number of master and slave DOFs in a finite element model (FEM) of the structure, respectively. As such, the rotational DOFs are considered slave DOFs, and therefore, the translational DOFs are regarded as master DOFs. The static condensation transformation matrix of the structure T is utilised to condense the slave DOFs in the structural siffness, mass, and damping matrices as follows [33]:

$$\bar{K} = T^{\mathrm{T}}\; K\; T \tag{4}$$

$$\bar{M} = T^{\mathrm{T}}\ M\ T \tag{5}$$

$$\bar{C} = T^{\mathrm{T}}\ C\ T \tag{6}$$

where

$$[T] = \begin{bmatrix} [I]_{m\times m} \\ -[K]^{-1}_{s\times s}[K]_{s\times m} \end{bmatrix} \tag{7}$$

In above equations, I denotes the identity matrix, K, M, and C represent respectively the structural stiffness, mass, and damping matrices, and $\bar{K}$, $barM$, and $\bar{C}$ denote respectively their condensed form. Therefore, the condensed FRF (CFRF) $\bar{H}$ of the structure is obtained as follows:

$$\bar{H}(\omega) = (-\omega^2\bar{M} + j\omega\ \bar{C} + \bar{K})^{-1} \tag{8}$$

Note that, in practice, $\bar{H}$ is obtained through excitation and measurement conducted upon the master DOFs of the structure.

2.2. Hilbert Transform

Modern signal processing methods use the Hilbert transform to interpret signals. The Hilbert transform can be applied to a signal that comply with the causality condition [34]. This holds for a signal whose value is zero at negative times, or it is independent of any events in the future. As such, the Hilbert transform of a causal signal is defined as follows:

$$\hat{h}(t) = \lim_{\epsilon\to 0}\frac{1}{\pi}\int_{|\tau-t|>\epsilon}\frac{h(\tau)}{t-\tau}\ d\tau, \tag{9}$$

where $\hat{h}(t)$ represents the Hilbert transform of the causal signal $h(t)$ which can be equivalently defined as the convolution of $h(t)$ with the signal $1/\pi t$. Also, the limit $|\tau - t| > \epsilon$ satisfies Cauchy principle value for the convolution integral [35]. The integral of (9) converges for a causal signal and thus the Hilbert transform becomes well-defined for such a signal.

In order to obtain the instantaneous amplitude, frequency, and phase of a complex signal, the Gabor's analytic signal $h_a(t)$ is constructed [36], the real and imaginary parts of which are $h(t)$ and $\hat{h}(t)$, respectively. As such,

$$h_a(t) = h(t) + j\hat{h}(t). \tag{10}$$

The Euler's representation of (10) is obtained as follows:

$$h_a(t) = h_m(t)\ e^{j\phi(t)}, \tag{11}$$

where $h_m(t)$ and $\phi(t)$ denote the time-variant "instantaneous amplitude" (IA) and "instantaneous phase" (IP) of the analytical signal $h_a(t)$, respectively, and can be obtained as follows:

$$h_m(t) = \sqrt{h^2(t) + \hat{h}^2(t)}, \tag{12}$$

$$\phi(t) = \tan^{-1}\left(\frac{\hat{h}(t)}{h(t)}\right). \tag{13}$$

The concept of instantaneous amplitude and frequency was employed successfully for damage detection in authors' previous work [31]. Sometimes, a continuous phase function is represented by unwrapped radian phases. As such, whenever a jump $\geq \pi$ radians between two consecutive angles presents, the angles are shifted by adding multiples of $\pm 2\pi$ until the jump is less than π. This is shown in Figure 2 more clearly where the x-axis is frequency instead of time (for

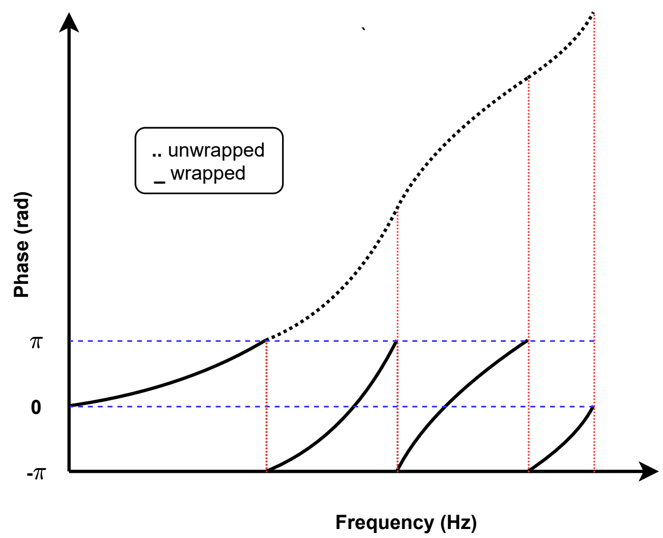

Figure 2: The wrapped and unwrapped instantaneous phase.

FRF/CFRF). Since, the concept of the unwrapped instantaneous Hilbert phase (UIHP) is informative about health condition of structures [37], the UIHP of the CFRF is proposed to be used, instead of the CFRF, for damage detection.

Since the definition of the instantaneous frequency, phase, and amplitude is only well-defined for a narrow-band signal, VMD is employed to extract narrow-band IMFs from each row of the CFRF, for which the UIHP is well-defined. The corresponding row of the CFRF is then replaced by the sum of all UIHPs (SUIHP) to obtain a new matrix to be used for damage detection using the proposed sensitivity-based model updating equation. As such, the SUIHP of a CFRF ($H(\omega)$) refers to the reconstructed CFRF matrix when its rows are replaced by their SUIHP obtained from the VMD decomposition and Gabor's analytical signal as discussed above and is shown as $\tilde{H}(\omega)$. Reiterated, in this paper, SUIHP can refer to a row of the obtained matrix or the entire matrix, depending on the context.

2.3. Variational mode decomposition (VMD)

The variational Mode Decomposition (VMD) algorithm is an adaptive signal decomposition method which decomposes a signal $f(t)$ into K narrow-band Amplitude-Modulated Frequency-Modulated (AM-FM) modes, termed Intrinsic Mode Functions (IMFs). An IMF can be thus written in the following form:

$$u_k(t) = A_k(t)\,\mathbf{cos}(\phi_k(t)), \tag{14}$$

where $u_k(t)$ is the k^{th} IMF, and $A_k(t)$ and $\phi_k(t)$ denote respectively its instantaneous frequency and phase. Since each IMF is narrow-band, the Gabor's analytical signal can be constructed for it, whereby the instantaneous phase can be also obtained. Each IMF is characterised by its center frequency ω_k. To calculate u_k and ω_k, VMD optimises the following augmented Lagrangian:

$$\begin{aligned}\mathcal{L}(\{u_k\},\{\omega_k\},\lambda) = \alpha \sum_k \left\| \partial_t \left(\delta(t) + \frac{j}{\pi t} * u_k(t) \right) \times e^{-j\omega_k t} \right\|_2^2 \\ + \left\| f(t) - \sum_k u_k(t) \right\|_2^2 + \left\langle \lambda(t), f(t) - \sum_k u_k(t) \right\rangle \end{aligned} \tag{15}$$

where $\|.\|_2$ is the L^2 norm, $*$ denotes convolution, and j is the imaginary unit. The penalty factor α is a denoising factor by factorising the importance of the first term with respect to the second and third terms in (15). Therefore, there are some parameters in the computer program of the VMD that need to be specified *a priori* [38]. These are listed as follows:

1. K, which determines the number of IMFs into which the original signal will be decomposed. In this paper, different numbers of K are chosen to see its effects on damage detection results.
2. α, which is a quadratic penalty term and is a denoising factor. In this paper, denoising is not intended through α, as specifying a value for α requires *a priori* knowledge about the percentage of noise in the CFRF matrix. As such, to make the value of α ineffective, the parameter τ (see below) is set to a small value, i.e. 0.1, as recommended by the proposers of the VMD algorithm [38].
3. τ, is a time step and determines how quickly the Lagrangian multiplier accumulates the reconstruction error. Setting τ to a small number, like 0.1, makes α, and thus denoising, ineffective.
4. ϵ, which is a tolerance parameter and controls the convergence of the algorithm. In this paper the value of 10^{-5} was selected for ϵ. Note that any value smaller than the specified value value, like $\epsilon = 10^{-}7$, did not further improve the results and only increased the convergence time of the computer program.
5. *init*, which initialises the centre frequencies. The options are zero ($init = 0$), uniform ($init = 1$), and random ($init = 2$). Since the way of initializing the center frequencies did not affect the final results [39], $init = 0$ was selected in this paper.
6. DC, which is a Boolean parameter determining whether or not the first mode is set and kept at DC (an IMF with zero center frequency). In this paper, DC was set to zero (false), however, setting DC at 1 would not affect the final results.

The VMD algorithm has been successfully employed for several purposes such as: (1) damage detection in beam type structures subjected to moving mass [31], (2) feature extraction of ultrasonic test results conducted on wood materials [40], and (3) denoising and removing seasonal patterns from signals used for condition monitoring of civil infrastructures [41, 42, 43].

3. The proposed sensitivity-based model-updating damage detection method

Sensitivity-based methods have been proven to be successful for damage detection of structures with closely-situated eigenvalues in some previous work such as [44]. Here, a method is proposed that can update the structural damage indices through developing a sensitivity-based equation that employs the concept of SUIHP.

Consider an n-DOF structure. The SUIHP of the CFRF obtained from the excitation of the structure at some DOFs and measurements made at some others is fed into a sensitivity-based model updating equation. In this section, the theoretical backgrounds of the so-called sensitivity-based model-updating problem leading to the proposed equation are discussed.

Consider a system excited by the force vector $\bar{F}(\omega_k)$ at its masters DOFs where ω_k is the k^{th} excitation frequency. Then, the measured response, at masters DOFs, of the real structure[2] can be written as:

$$\bar{X}_m\left(\alpha, \omega_k\right) = \bar{H}_m\left(\alpha, \omega_k\right) \bar{F}\left(\omega_k\right) \tag{16}$$

where $\bar{X}_{\mathrm{m}}\left(\alpha, \omega_k\right)$ is the measured structural response vector. Likewise, for a numerical FEM[3], one can write:

$$\bar{X}_c\left(\hat{\alpha}, \omega_k\right) = \bar{H}_c\left(\hat{\alpha}, \omega_k\right) \bar{F}\left(\omega_k\right) \tag{17}$$

where $\bar{X}_{\mathrm{c}}\left(\hat{\alpha}, \omega_k\right)$ is the response vector of the FEM based on $\hat{\alpha}$, i.e. the estimated value of the vector of damage indices α. $\bar{H}_m\left(\alpha, \omega_k\right)$ and $\bar{H}_c\left(\hat{\alpha}, \omega_k\right)$ denote the CFRFs obtained from the real

[2] In this paper, the real structure refers to the FEM with a simulated damage scenario.
[3] The to-be-updated FEM model.

model and the estimated FEM, respectively. Hence, the error associated with this estimation is a function of $\hat{\alpha}$ and is defined as the L^2 norm of the difference between the measured and computed structural responses as follows:

$$J(\hat{\alpha}) = \left\|\epsilon\right\|_2^2 = \left\|\bar{X}_{\mathrm{m}}(\alpha,\omega_k) - \bar{X}_{\mathrm{c}}(\hat{\alpha},\omega_k)\right\|_2^2 \tag{18}$$

where $J(\hat{\alpha})$ is the error function of the estimated vector of unknowns, i.e. $\hat{\alpha}$. ϵ denotes the residual vector obtained from the difference between the measured and updated responses.

A truncated (first-order) Taylor series expansion of (18) can be written as follows:

$$\bar{X}_{\mathrm{m}}(\alpha,\omega_k) \simeq \bar{X}_{\mathrm{c}}(\hat{\alpha},\omega_k) + \frac{\partial \bar{X}_{\mathrm{c}}(\hat{\alpha},\omega_k)}{\partial \hat{\alpha}}\,\delta\hat{\alpha} \tag{19}$$

The derivative of the computed response vector $\bar{X}_{\mathrm{c}}(\hat{\alpha},\omega_k)$ with respect to the estimated unknowns vector of $\hat{\alpha}$ can be written as follows [18]:

$$\begin{aligned}\frac{\partial \bar{X}_{\mathrm{c}}(\hat{\alpha},\omega_k)}{\partial \hat{\alpha}} &\simeq -\bar{H}_{\mathrm{c}}(\hat{\alpha},\omega_k)\\ &\times\left(-\omega^2\frac{\partial \bar{M}}{\partial \hat{\alpha}} + j\omega\frac{\partial \bar{C}}{\partial \hat{\alpha}} + \frac{\partial \bar{K}}{\partial \hat{\alpha}}\right)\bar{X}_{\mathrm{c}}(\hat{\alpha},\omega_k)\end{aligned} \tag{20}$$

Substituting Eq. 20 into Eq. 19 results in the following equation:

$$\begin{aligned}\epsilon &= \bar{X}_{\mathrm{m}}(\alpha,\omega_k) - \bar{X}_{\mathrm{c}}(\hat{\alpha},\omega_k)\\ &\simeq \Big[-\bar{H}_{\mathrm{c}}(\hat{\alpha},\omega_k)\left(-\omega^2\frac{\partial \bar{M}}{\partial \hat{\alpha}} + j\omega\frac{\partial \bar{C}}{\partial \hat{\alpha}} + \frac{\partial \bar{K}}{\partial \hat{\alpha}}\right)\\ &\times \bar{X}_{\mathrm{c}}(\hat{\alpha},\omega_k)\Big]\,\delta\hat{\alpha}\end{aligned} \tag{21}$$

It is obvious that since (21) is obtained by neglecting the higher order of Taylor series expansion, it only provides an approximate solution. However, the higher terms are expected to have minimal effects on the final results [18, 44].

One can write the measured CFRF $\bar{H}_{\mathrm{m}}(\alpha,\omega_k)$ in terms of the perturbed structural stiffness, mass, and damping matrices as follows:

$$\bar{H}_{\mathrm{m}}(\alpha,\omega_k) = \left(-\omega^2(M+\delta M) + j\omega(C+\delta C) + K + \delta K\right)^{-1} \tag{22}$$

where

$$\delta\bar{K} = \sum_{i=1}^{n}\frac{\partial \bar{K}}{\partial \hat{\alpha}_{\mathrm{i}}}\delta\hat{\alpha}_{\mathrm{i}} \tag{23}$$

$$\delta\bar{M} = \sum_{i=1}^{n}\frac{\partial \bar{M}}{\partial \hat{\alpha}_{\mathrm{i}}}\delta\hat{\alpha}_{\mathrm{i}} \tag{24}$$

The changes of the structural response, in terms of the measured CFRF, thus can be written as follows [18]:

$$\begin{aligned}\delta\bar{X}_{\mathrm{c}}(\hat{\alpha},\omega_k) &\simeq -\bar{H}_{\mathrm{m}}(\alpha,\omega_k)\\ &\times\left(-\omega_k^2\delta\bar{M} + j\omega_k\delta\bar{C} + \delta\bar{K}\right)\bar{X}_{\mathrm{c}}(\hat{\alpha},\omega_k)\end{aligned} \tag{25}$$

Substituting (23) and (24) into (25) and writing the obtained equation in a compact form, we have:

$$\delta\bar{X}(\hat{\alpha},\omega_k) \simeq \begin{bmatrix} S^{\bar{K}} & S^{\bar{M}} \end{bmatrix}\begin{bmatrix}\delta\hat{\alpha}\\ \delta\hat{\alpha}\end{bmatrix} \tag{26}$$

where

$$S^{\bar{K}} = \left[-\bar{H}_{\rm m}(\alpha,\omega_k)\left(\frac{\partial \bar{K}}{\partial \hat{\alpha}_1}\right)\bar{X}_{\rm c}(\hat{\alpha},\omega_k), \ldots, -\bar{H}_{\rm m}(\alpha,\omega_k)\left(\frac{\partial \bar{K}}{\partial \hat{\alpha}_n}\right)\bar{X}_{\rm c}(\hat{\alpha},\omega_k)\right] \tag{27}$$

and

$$S^{\bar{M}} = \left[-\bar{H}_{\rm m}(\alpha,\omega_k)\left(\frac{\partial \bar{M}}{\partial \hat{\alpha}_1}\right)\bar{X}_{\rm c}(\hat{\alpha},\omega_k), \ldots, -\bar{H}_{\rm m}(\alpha,\omega_k)\left(\frac{\partial \bar{M}}{\partial \hat{\alpha}_n}\right)\bar{X}_{\rm c}(\hat{\alpha},\omega_k)\right] \tag{28}$$

Note that in this paper the SUIHP of the CFRF, shown as $\tilde{H}(\alpha,\omega_k)$, is used as opposed to $\bar{H}(\alpha,\omega_k)$ in (27) and (28). The least square (LS) method is employed to solve (26) in iterations. As such, the value of $\hat{\alpha}$ at the $t^{\rm th}$ iteration ($\hat{\alpha}_t$) is updated as $\hat{\alpha}_t = \hat{\alpha}_{t-1} + \delta\hat{\alpha}_t$. Note that $\delta\hat{\alpha}_t$ represents an incremental update acquired for α through running the LS algorithm for solving the optimisation problem at time t.

It was set for the algorithm to terminate iterations when $|\delta\hat{\alpha}_t| \leq 10^{-5}$. The SUIHP of the CFRF is relatively a slowly varying function. Hence, a larger number of iterations might be required for (28) to converge to a solution.

4. The effective arrangement of the excitation frequency ranges and locations

4.1. Proper selection of the excitation frequency ranges

FRF-based model updating methods require excitation of appropriate frequency ranges. As such, frequency ranges that are more sensitive to the variation of the structural parameters are desirable. A previous study recommends that the excitation frequency ranges close to the resonant frequencies should be used to this end [15]. Accordingly, there are two reasons that such frequency ranges are of interest. These are:

1. To increase the sensitivity of the structural response to any small variation of the structural parameters.
2. To reduce the effect of damping on the structural response.

However, there is a catch; one needs to minimise the effect of damping on the structural response. This is mainly due to the fact that an exact, or close to exact, simulation of the structural damping in the FEM is difficult in most of the cases. It is known that the effect of damping on FRF reduces as excitation ranges are selected far enough from resonances [18]. Therefore, there are optimal frequency ranges for excitation to satisfy all the above, although these frequency ranges need to be identified for each case individually. In this paper, CFRFs obtained from different frequency ranges are concatenated to obtain a uniform CFRF matrix.

Note that since the damage indices are updated in each iteration, the computed CFRF matrix $\bar{H}_{\rm c}(\alpha,\omega_k)$ corresponding to the to-be-updated model shifts slightly at each iteration. This demands for the update of $H_{\rm c}(\omega)$ at each iteration which is done through an automated frequency-range-selection program based on the aforementioned rules. For further information the readers are referred to [19, 18, 15].

4.2. Proper selection of the excitation locations

The proper selection of the excitation locations plays an important role in obtaining accurate results regarding the model-updating problem as well [45]. Hence, in this section, a method is proposed based on the obtained SUIHP of the CFRF matrix of the FEM at each iteration. The proposed method is obtained through replacing $\bar{H}_{\rm m}(\hat{\alpha},\omega_k)$ by its SUIHP shown by $\tilde{H}_{\rm m}(\hat{\alpha},\omega_k)$ [15] that will avoid obtaining a rotational DOF among the obtained optimum excitation DOFs. As such, the proposed equation for identifying optimal locations of excitation is written as follows:

$$\tilde{\Lambda} = \sum_{k=1}^{K} \sqrt{\sum_{i=1}^{n} \left(\tilde{H}_{{\rm m},ij}(\hat{\alpha},\omega_k)\right)^2} \tag{29}$$

where K is the number of excitation frequencies. The ne DOFs corresponding to the highest values of $\tilde{\Lambda}$ are selected as the best excitation locations. Note that, despite the previous section, the excitation locations are not updated in each iteration and are identified only once, based on the numerical model corresponding to the intact structure.

Note that in this paper, the matrix of the CFRF $\bar{H}_{\mathrm{m},ij}(\hat{\alpha}, \omega_k)$, and therefore $\tilde{H}_{\mathrm{m},ij}(\hat{\alpha}, \omega_k)$, is obtained through excitation of the identified optimum DOFs and measurements conducted on all the translational DOFs.

5. Damage identification accuracy indicators

Three accuracy indicators are employed to asses the accuracy of the results of the damage detection using the proposed method [10]. These are listed as follows:

1. The closeness index (CI) is employed to evaluate the accuracy of the predicted damage indices. It is defined based on the difference between the actual and the computed vectors of damage indices as follows:

$$\mathrm{CI} = 1 - \frac{\|P^r - P^c\|_2}{\|P^r\|_2} \tag{30}$$

   where P^r and P^c indicate the vectors of real and computed damage indices, respectively. Accordingly, CI $= 1$ implies that all the updated parameters are exact.
2. The mean sizing error (MSE) is defined as the sum of the absolute difference between the real and computed damage parameters normalized by the number of real damaged elements de as follows:

$$\mathrm{MSE} = \frac{1}{de}\sum_{e=1}^{de}|p_e^r - p_e^c|, \quad 0 \leq \mathrm{MSE} \tag{31}$$

   where p_e^r and p_e^c denote respectively the real and computed damage parameters of the e^{th} element.
3. The relative error RE is defined as follows:

$$\mathrm{RE} = \frac{\sum_{e=1}^{n}|p_e^r| - \sum_{e=1}^{n}|p_e^c|}{\sum_{e=1}^{n}|p_e^c|}, \quad -1 \leq \mathrm{RE} \leq 1 \tag{32}$$

   where n is the number of all elements (damaged and intact) in the FEM of the structure. Smaller values of the MSE and RE imply a more accurate prediction.

The flowchart of the proposed method is depicted in Fig. 3.

6. Numerical examples

The properties of the composite plate studied in this section is adopted from [46]. It is a fixed supported square laminated composite plate with different number of layers (NoL) and layering angles (LA) as follows:

- NoL = 3 and LA = 0°/90°/0°,
- NoL = 6 and LA = 0°/45°/0°/0°/45°/0°.

The specifications of the plates under study are listed as follows:

- The size of the plates is $100 \times 100 \times 10$ cm. As such, the overall thickness of the plate was considered 10 cm regardless of the number of layers.

https://doi.org/10.1016/j.compstruct.2022.115243

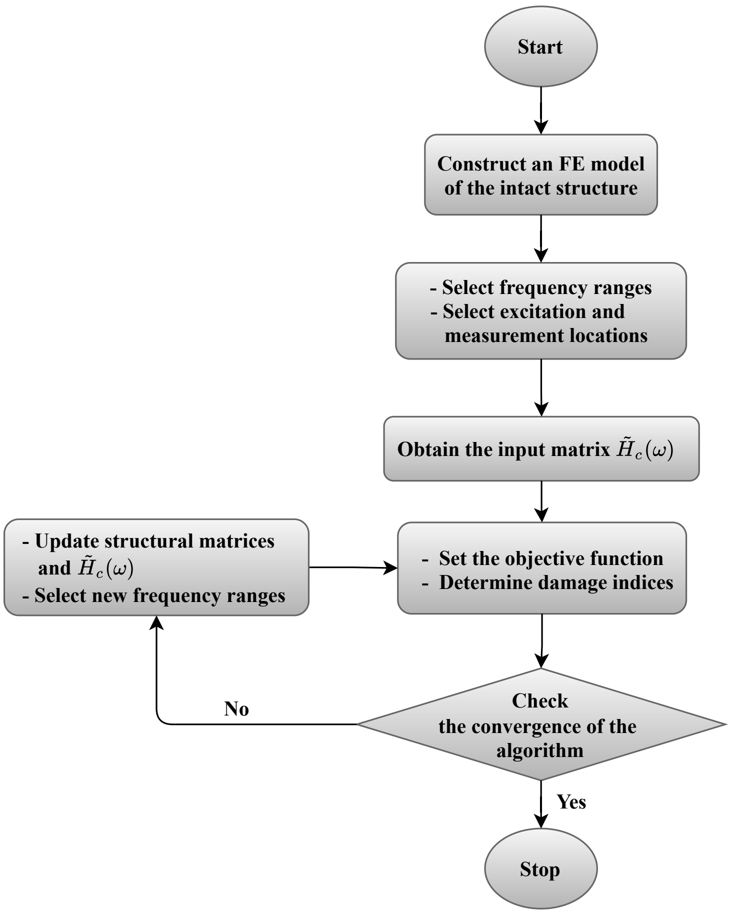

Figure 3: The flowchart of the proposed sensitivity based model-updating method.

Table 1: The material properties of each ply in the composite laminate plate adopted from [46]
.

Young's Modulus	Young's Modulus	Poisson ratio	Poisson ratio	Modulus of rigidity	Modulus of rigidity
E_1 (N/m^2)=40	E_2 (N/m^2)=1	ν_{12}=0.25	ν_{21}=0.00625	$G_{12} = G_{13} = 0.6E_2$	$G_{23} = 0.5E_2$

- The plates are divided into $n_x \times n_y$ four-node elements with a total number of $(n_x + 1) \times (n_y + 1)$ nodes (see Fig. 4a). Note that n_x and n_y indicate the number of divisions along the x and y axes, respectively (Fig. 4b).
- As a result, the plates are divided into 36 elements with a total of 245 DOFs ($n_x = n_y = 6$). These include three translational and two rotational DOFs at each node.
- The four sides of the plates are fixed supported and, therefore, 125 DOFs remain active.

An in-house MATLAB code was developed for the simulation of the composite plates and solving the problem of damage detection via the proposed method. The first-order shear deformation theory (FSDT), that extends the kinematics of the Classical Laminated Plate Theory (CLPT) [46], was employed for the simulation of the laminated composite structures of this study. Table 1 lists all the mechanical properties of each layer of the plates under study in this paper. Note that the plates under study are identical to the ones studied in [12, 20, 47, 48, 49, 50], in terms of the geometry and boundary conditions. Several damage scenarios have been considered as listed in Table 2. These are six different damage scenarios based on the location, severity and the type of damage. Damage is considered as a degradation factor introduced to the elemental stiffness (stiffness reduction). Table 3 lists the 10 lowest natural frequencies of the plates with

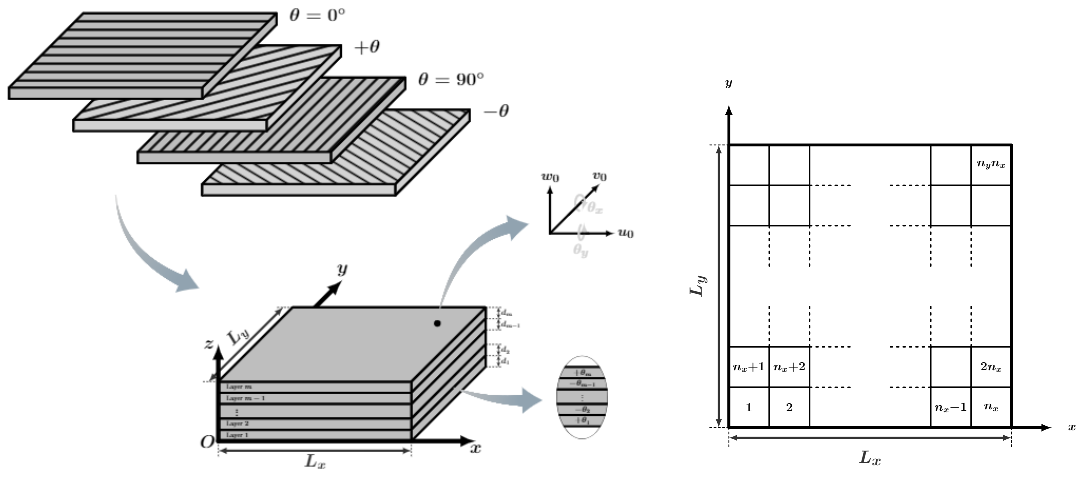

(a) (b)

Figure 4: (a) The sketch of the composite laminate plate, and (b) the element numbering of the composite laminate plate ($n_x = n_y = 6$).

Table 2: Damage scenarios of the composite laminate plate.

Case 1		Case 2		Case 3		Case 4		Case 5		Case 6	
Element	Ratio	Element	Ratio	Element	Ratio	Element	Ratio	Element	Ratio	Element	Ratio
5	0.20	2	0.15	1	0.20	5	0.15	4	0.15	3	0.20
12	0.30	10	0.20	10	0.15	10	0.10	8	0.20	7	0.15
24	0.15	15	0.25	12	0.10	15	0.20	17	0.30	9	0.10
31	0.20	25	0.30	13	0.20	20	0.25	23	0.15	19	0.30
		31	0.20	17	0.30	25	0.30	31	0.10	23	0.35
				29	0.25	30	0.10	36	0.20	31	0.20

different damage scenarios. It is evident from the table that reducing the stiffness brings about decreasing the natural frequencies of all models of the plate. Note that here only the first 10 natural frequencies of the studied plate models are presented. The small difference between these modes justifies the almost similar effect of the damage on them. This is due to the closely-situated-eigenvalues property of the studied composite plates which was fully investigated in some previous work such as [44, 51].

It is known that structures with many DOFs, such as spatial truss and plate structures, can have many closely-situated eigenvalues [52]. This can, however, result in missing information about damage due to the semi-repeated modes. As such, higher modes are required to be identified to compensate for the loss of information from the semi-repeated lower modes. However, measuring higher modes is also usually troublesome, making the damage detection of such structures relatively more challenging [53, 51]. We will show that the plates under study in this section have a few number of closely-situated eigenvalues. However, to characterise the closeness of the eigenvalues in a structure, a metric is presented in here which is developed based on a similar concept introduced in [53] for damped structures as follows:

Consider two successive structural natural frequencies of $\omega_1 = \omega$ and $\omega_2 = \omega + \Delta\omega$. These are considered closely-situated frequencies if $\Delta\omega = \omega_2 - \omega_1$ is relatively small compared to ω [51]. To characterise this further, the frequency relative disparity (FRD) index, for two adjacent frequencies is introduced as follows:

$$\mathrm{FRD}_{1,2}\% = \left| \frac{\omega_2 - \omega_1}{\omega_1} \right| \times 100. \tag{33}$$

As such, different scenarios can hold for two successive modes as follows [53]:

Table 3: First ten natural frequencies of the composite laminate plate with different NoL and LA.

Lamination scheme		Mode No. 1	2	3	4	5	6	7	8	9	10
Intact	NoL = 3, LA = (0°/90°/0°)	7.40	11.14	14.32	16.23	18.74	21.42	23.32	23.90	25.74	26.29
	NoL = 6, LA = (0°/45°/0°)	7.64	11.53	14.74	16.82	19.07	21.99	23.78	24.90	25.78	26.60
Case 1	NoL = 3, LA = (0°/90°/0°)	7.30	11.01	14.11	15.92	18.61	21.08	23.08	23.58	25.39	25.92
	NoL = 6, LA = (0°/45°/0°)	7.55	11.42	14.55	16.48	19.01	21.53	23.54	24.68	25.46	26.40
Case 2	NoL = 3, LA = (0°/90°/0°)	7.32	10.94	14.07	15.85	18.44	21.03	22.95	23.42	25.34	25.89
	NoL = 6, LA = (0°/45°/0°)	7.55	11.34	14.50	16.45	18.74	21.50	23.41	24.53	25.44	26.31
Case 3	NoL = 3, LA = (0°/90°/0°)	7.24	10.96	14.03	15.96	18.50	21.03	22.73	23.47	25.26	25.79
	NoL = 6, LA = (0°/45°/0°)	7.47	11.33	14.45	16.55	18.82	21.54	23.26	24.42	25.31	26.02
Case 4	NoL = 3, LA = (0°/90°/0°)	7.27	10.94	14.06	15.85	18.46	21.01	22.80	23.43	25.34	25.88
	NoL = 6, LA = (0°/45°/0°)	7.52	11.33	14.49	16.41	18.83	21.48	23.28	24.50	25.42	26.31
Case 5	NoL = 3, LA = (0°/90°/0°)	7.28	10.99	14.22	16.06	18.45	21.05	22.92	23.61	25.33	25.85
	NoL = 6, LA = (0°/45°/0°)	7.52	11.35	14.63	16.62	18.80	21.61	23.40	24.54	25.39	26.14
Case 6	NoL = 3, LA = (0°/90°/0°)	7.19	10.94	13.95	15.92	18.43	20.99	22.67	23.50	25.10	25.80
	NoL = 6, LA = (0°/45°/0°)	7.43	11.29	14.40	16.51	18.68	21.67	23.18	24.37	25.19	25.98

- Well-separated: $\mathrm{FRD}_{1,2} > 10\%$,
- Separated modes: $5\% < \mathrm{FRD}_{1,2} \leq 10\%$,
- Close modes: $1\% < \mathrm{FRD}_{1,2} \leq 5\%$, and
- very close modes: $\mathrm{FRD}_{1,2} \leq 1\%$.

Fig. 5 shows examples of the CFRFs obtained from the composite laminate plates when the plates are excited at the DOF 21 and measured at the DOF 12. There are a number of closely-situated eigenvalues marked in the graphs. However, as can be seen, it is hard to distinguish the closely-situated eigenvalues by visual inspection of the CFRFs. Table 4 presents the FRD metric computed for the first ten modes of the structures to better characterise the closely-situated eigenvalues. Reiterated, the existence of the closely-situated eigenvalues makes the task of the damage detection of the plate using modal information challenging. Therefore, using FRFs (CFRFs in this paper) seems more reasonable. We show further that the proposed SUIHP does even a better job compared to the CFRF, when the CFRF data are highly contaminated by measurement noise.

6.1. Considering the effect of noise

It is crucial to study the effect of the measurement noise on the performance of damage detection methods. Therefore, the simulated structural CFRF data are contaminated by different level of noise through the following formula [54]:

$$\hat{\delta} = \delta + \frac{NP}{100}\, n_{noise}\, \sigma(\delta) \tag{34}$$

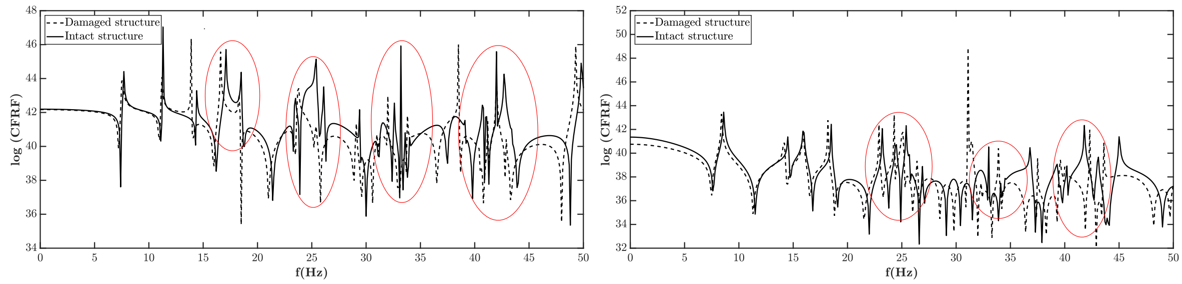

(a) NoL = 3 and LA = 0°/90°/0°

(b) NoL = 6 and LA = 0°/45°/0°/0°/45°/0°

Figure 5: The closely-situated natural frequencies of the intact and damaged composite laminate plate with different arrangements (damage scenario 1, excited at DOF 21 and measured at DOF 12).

Table 4: The $\mathrm{FRD}_{i,j}$ values for the first ten modes of the composite laminate plate with different NOLs and LAs.

Mode No.	Closely spaced modes with lamination scheme			
	NoL = 3, LA = 0°/90°/0°		NoL = 6, LA = 0°/45°/0°/0°/45°/0°	
	$\mathrm{FRD}_{i,j}$ (%)	Modal disparity	$\mathrm{FRD}_{i,j}$ (%)	Modal disparity
[1, 2]	50.54	Well-separated	50.92	Well-separated
[2, 3]	28.55	Well-separated	27.84	Well-separated
[3, 4]	13.33	Well-separated	14.11	Well-separated
[4, 5]	15.46	Well-separated	13.37	Well-separated
[5, 6]	14.30	Well-separated	15.31	Well-separated
[6, 7]	8.87	Separated	8.40	Separated
[7, 8]	2.48	Close	4.70	Close
[8, 9]	7.69	Separated	3.49	Close
[9, 10]	2.14	Close	3.22	Close
[10, 11]	12.00	Well-separated	1.69	Close

where δ and $\hat{\delta}$ indicate the simulated clean and noisy CFRF data with standard deviation $\sigma(\delta)$. As such, NP is the noise percentage which is set at 30 in this paper, and n_{noise} is a random vector sampled from the standard normal distribution.

Fig. 6 shows the examples of the obtained noisy CFRF signals from the excitation and measurement of the composite laminate plates at some translational DOFs.

6.2. The proper selection of the Excitation location

Proper selection of the excitation location has a great effect on the damage detection results. There are three directions for the translational DOFs in the global coordinates in all the nodes of an element; these DOFs are marked in this paper as DOFs_t^1, DOFs_t^2, and DOFs_t^3. The DOFs corresponding to the optimum excitation location are selected through calculation of $\tilde{\Lambda}$ in Eq.29.

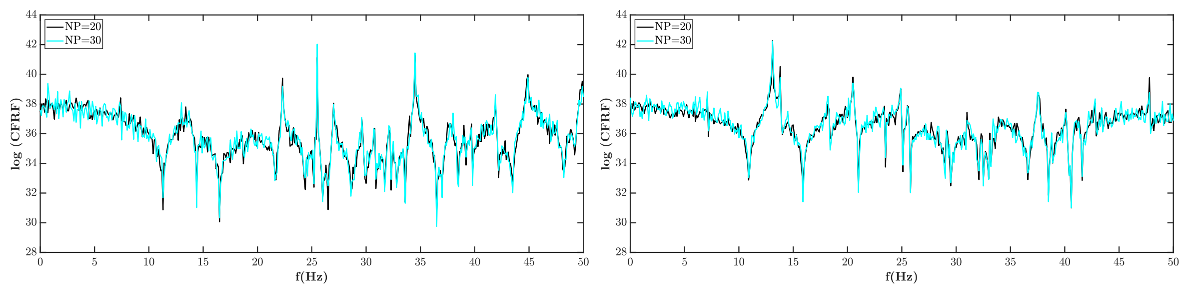

(a) NoL = 3 and LA = 0°/90°/0°

(b) NoL = 6 and LA = 0°/45°/0°/0°/45°/0°

Figure 6: The obtained noisy CFRF corresponding to the composite laminate plate with different arrangements (for the 1st damage scenario, excited at DOF 21 and measured at DOF 72).

Table 5: The optimal excitation locations obtained for the laminated composite plate with different configurations.

Plate	S_j	**DOFs**
NoL = 3, **LA** = (0°/90°/0°)	25.24, 23.65, 20.19, 17.25, 17.23, 17.05, 16.25	71, 66, 56, 31, 101, 47, 72
NoL = 6, **LA** = (0°/45°/0°/0°/45°/0°)	34.07, 33.74, 33.22, 32.08, 27.25, 22.54, 18.25	21, 66, 31, 41, 107, 117,122

Accordingly, the highest values of $\tilde{\Lambda}$ was obtained at the first and second transitional DOFs, as shown in Table 5. The table lists the obtained optimum locations of excitation for the two models of the composite plate. As such, the number of identified optimal locations for excitation presented here is equal to eight. The fact that the identified optimal DOFs are among the first and second translational DOFs may be somewhat sensible through a preliminary study of the elemental information. However, one should note that the total number of the first and second DOFs in the simulated plates is equal to 50. Therefore, identifying optimal excitation locations is crucial for saving the time of the experiment as well as ensuring accurate results for damage detection. In practical applications, plates can be excited by patches of piezoelectric actuator at the identified optimal locations [55]. Different sensing technologies can be employed for the measurement of the structural response to the excitation force such as accelerometers, optic fiber sensing technologies, automated laser total station, and 3D laser scanning, to name a few [56].

6.3. The effect of the number of decomposition

Fig. 7 depicts the obtained SUIHP signals when the structures are excited and measured at the translational DOFs 21 and 12, respectively. The SUIHP signals were obtained for both of the intact and damaged (4th damage scenario) structures. To investigate the sensitivity of the obtained SUIHP to the number of IMFs, different numbers of the modes (NOM) (decompositions) has been considered in the VMD settings which are 4, 6, and 8 decompositions.

The subplotes of Fig. 7 show that the maximum variability of the SUIHP, across different health conditions of the structure for different NOMs. A close examination of the plots suggest that more accurate results are expected to be achieved through optimising the objective function when NOM=4 is used for obtaining SUIHP of the CFRF. It is generally known that over-decomposing a signal using VMD can result in repetitive modes which can compromise the variability of the obtained SUIHP with respect to the damage. Moreover, under-decomposition of the rows of the CFRF can result in missing information about damage. This has been tested by setting NOM=3, the results of which is not presented in here. In a general case when the optimum number of the decomposition is concerned, one can start off with a small number, like NOM=3, and increase the number of the decomposition gradually. One can judge the optimum number of the decomposition through monitoring of the variability of the SUIHP of the damaged structure with respect to its value corresponding to the healthy state of the structure. Following, we will show that even a non-optimal number of decomposition, i.e. 6 and 8 in here, will bring about more accurate results compared to the case when the CFRF is used for damage detection.

In order to demonstrate the superiority of the proposed method both of the SUIHP and CFRF matrices were used for damage detection in this section. Also, although we showed that the variability of the SUIHP is more significant when NOM is equal to 4, the results obtained from other numbers of decomposition, i.e. NOM=6 and 8, are presented in this section. In order to consider the effect of the measurement noise on the results, the rows of the CFRF were contaminated by 30% random noise (NP=30). The obtained results of the damage detection conducted on different models of the composite plate and damage scenarios, using CFRF and SUIHP, are listed in Table 6. The results indicate that using SUIHP , regardless the number of NOM, brings about far more accurate results compared with the CFRF in all cases.

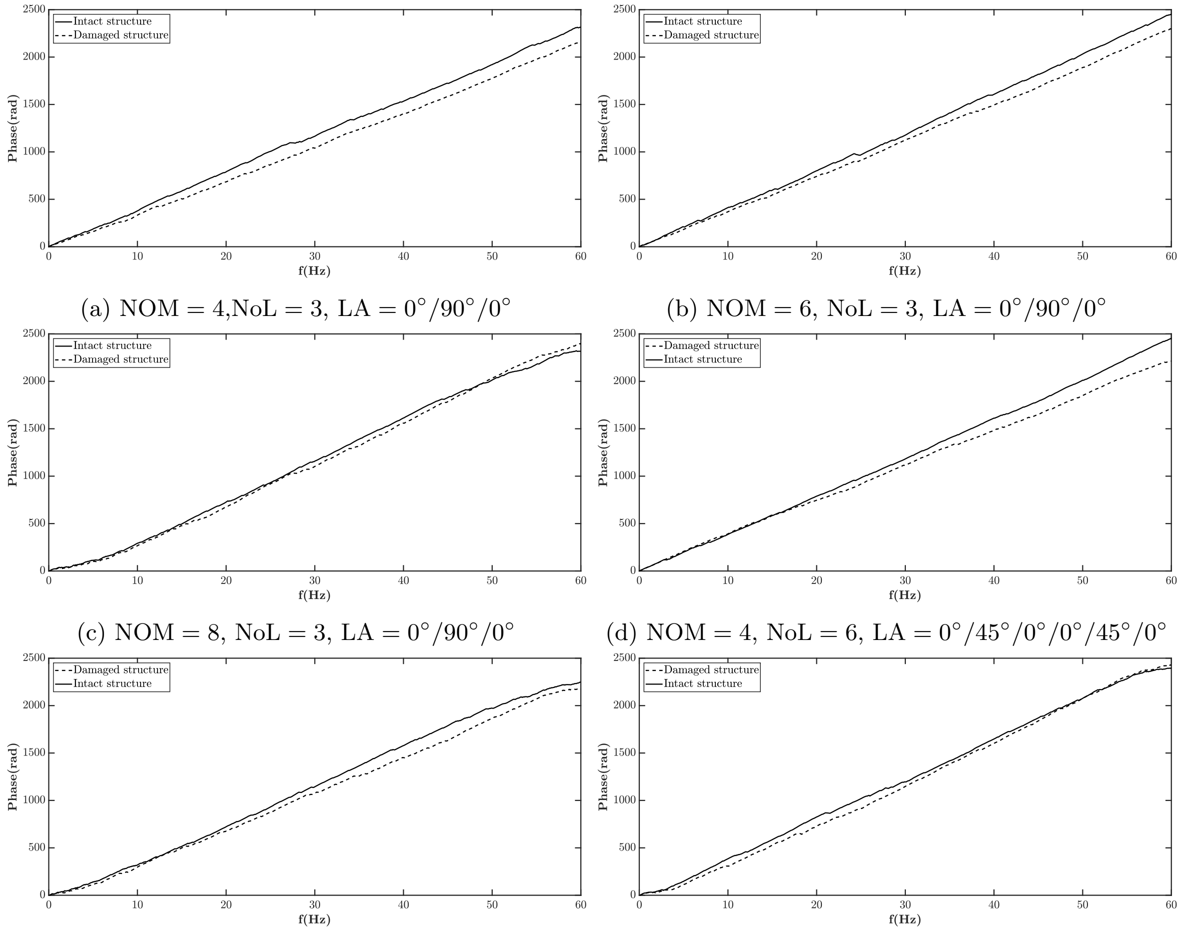

(a) NOM = 4,NoL = 3, LA = 0°/90°/0°

(b) NOM = 6, NoL = 3, LA = 0°/90°/0°

(c) NOM = 8, NoL = 3, LA = 0°/90°/0°

(d) NOM = 4, NoL = 6, LA = 0°/45°/0°/0°/45°/0°

(e) NOM = 6, NoL = 6, LA = 0°/45°/0°/0°/45°/0°

(f) NOM = 8, NoL = 6, LA = 0°/45°/0°/0°/45°/0°

Figure 7: The SUIHP of the damaged and healthy composite laminate for all studied models (damage scenario 4 , excited at DOF 21 and measured at DOF 12). Note that $f = \omega/2\pi$.

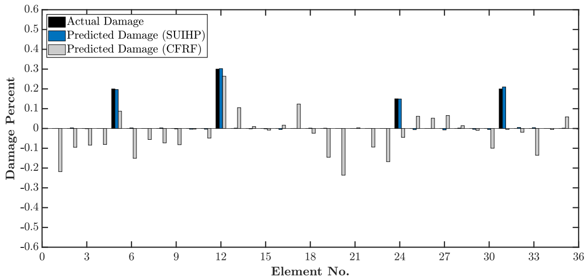

(a) Case 1

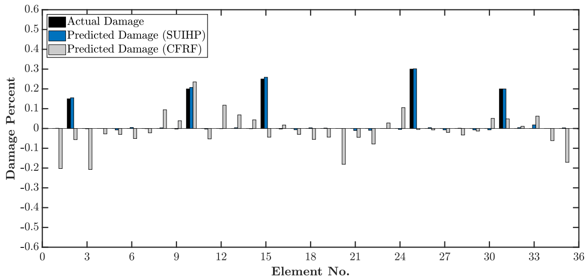

(b) Case 2

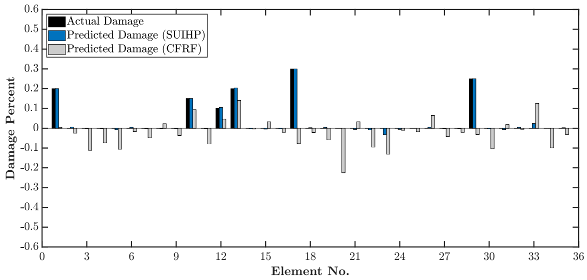

(c) Case 3

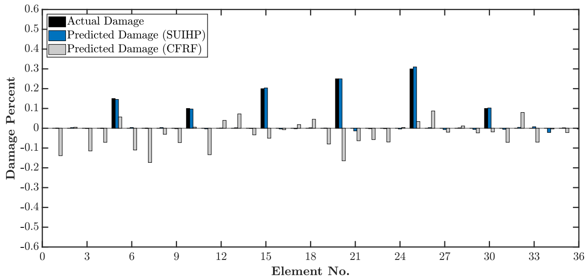

(d) Case 4

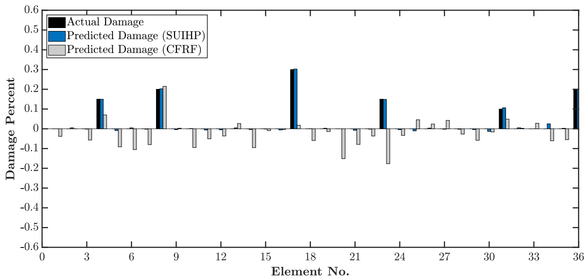

(e) Case 5

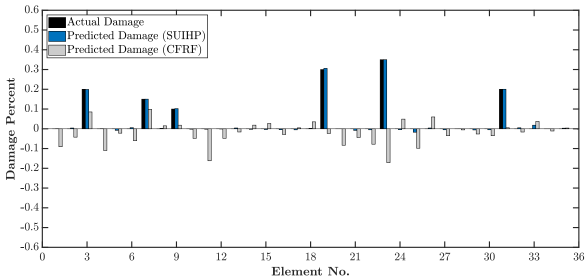

(f) Case 6

Figure 8: The predicted damage indices using CFRF and SUIHP in the proposed sensitivity based model-updating method for damage scenarios 1-6 in three-layer (0°/90°/0°) composite laminate plate and NP=30)

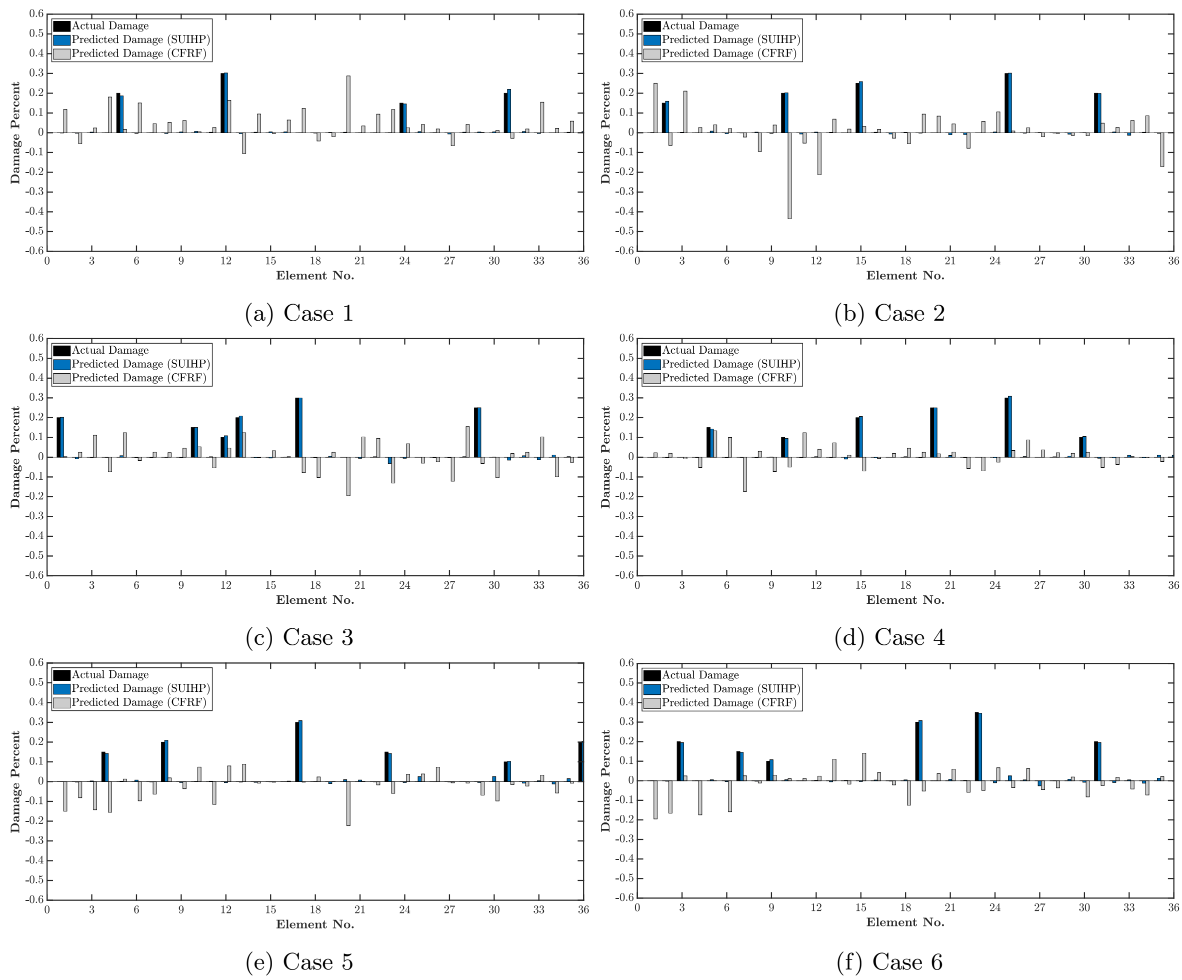

(a) Case 1 (b) Case 2

(c) Case 3 (d) Case 4

(e) Case 5 (f) Case 6

Figure 9: The predicted damage indices using CFRF and SUIHP in the proposed sensitivity based model-updating method for damage scenarios 1-6 in six-layer (0°/45°/0°) composite laminate plate (NP=30)

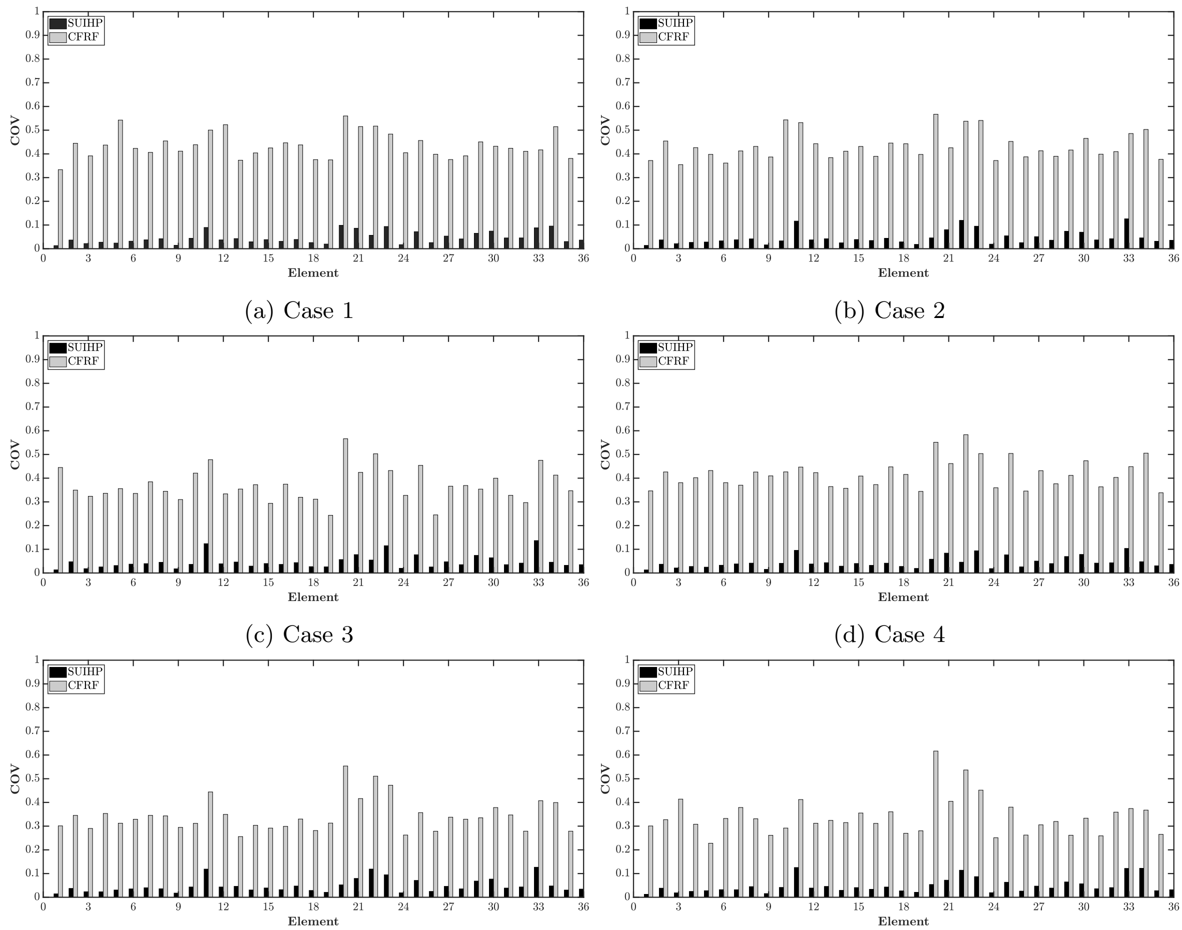

(a) Case 1

(b) Case 2

(c) Case 3

(d) Case 4

(e) Case 5

(f) Case 6

Figure 10: The COVs indices using CFRF and SUIHP in the proposed sensitivity based model-updating method for damage scenarios 1-6 in three-layer (0°/90°/0°) composite laminate plate (NP=30).

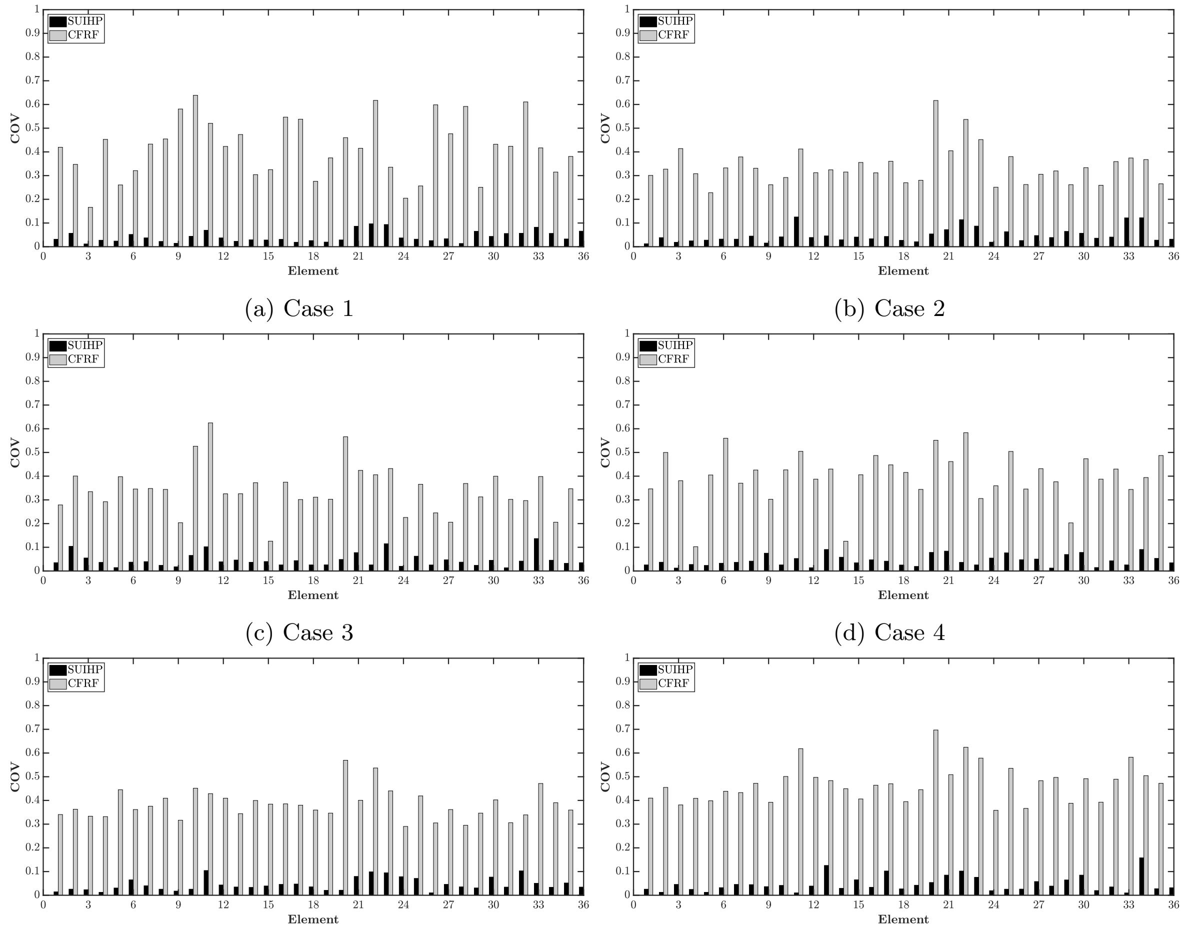

(a) Case 1 (b) Case 2

(c) Case 3 (d) Case 4

(e) Case 5 (f) Case 6

Figure 11: The COVs indices using CFRF and SUIHP in the proposed sensitivity based model-updating method for damage scenarios 1-6 in six-layer (0°/45°/0°) composite laminate plate (NP=30).

Table 6: Summary of the obtained error indices using the proposed sensitivity-based model-updating method for all damage cases in the studied composite laminate plates with different NOM.

Case No.	Applied method	NOM	NoL = 3, LA = (0°/90°/0°) MSE	RE	CI	NoL = 6, LA = (0°/45°/0°) MSE	RE	CI
1	CFRF	-	0.0807	-2.2453	-0.4216	0.0795	-1.8502	-0.4206
1	SUIHP	4	0.0024	-0.0931	0.9545	0.0037	-0.1158	0.9275
1	SUIHP	6	0.0312	-0.2569	2.7075	0.0423	-0.2963	2.9635
1	SUIHP	8	0.0512	-0.4103	3.3027	0.0712	-0.4001	3.0215
2	CFRF	-	0.0838	-1.1956	-0.3610	0.0994	-1.4139	-0.8410
2	SUIHP	4	0.0040	-0.1321	0.9349	0.0036	-0.1145	0.9423
2	SUIHP	6	0.0415	-0.3014	1.9980	0.0526	-0.3856	3.0247
2	SUIHP	8	0.0712	-0.6056	3.4360	0.0798	-0.6996	3.9125
3	CFRF	-	0.0770	-0.7856	-0.2929	0.0865	-0.9681	-0.3583
3	SUIHP	4	0.0044	-0.1312	0.9101	0.0046	-0.1377	0.9111
3	SUIHP	6	0.0185	-0.2703	2.1041	0.0376	-0.3107	3.1174
3	SUIHP	8	0.0368	-0.7002	3.4360	0.0498	-0.3906	3.9085
4	CFRF	-	0.0830	-0.8906	-0.4516	0.0643	-0.4848	-0.1775
4	SUIHP	4	0.0039	-0.1154	0.9306	0.0037	-0.0981	0.9394
4	SUIHP	6	0.0236	-0.3974	1.9001	0.0291	-0.4197	2.0010
4	SUIHP	8	0.0378	-0.5056	3.0760	0.0479	-0.4630	3.5569
5	CFRF	-	0.0655	-0.7950	-0.2150	0.0803	-0.8226	-0.4332
5	SUIHP	4	0.0043	-0.1364	0.9201	0.0059	-0.1639	0.8934
5	SUIHP	6	0.0352	-0.2874	2.3001	0.0423	-0.3002	2.6984
5	SUIHP	8	0.0421	-0.4126	3.7890	0.0498	-0.4556	3.4298
6	CFRF	-	0.0731	-0.5427	-0.2819	0.0893	-0.5951	-0.3515
6	SUIHP	4	0.0040	-0.1104	0.9399	0.0059	-0.1356	0.9130
6	SUIHP	6	0.0240	-0.3214	2.2149	0.0229	-0.3075	2.0369
6	SUIHP	8	0.0412	-0.5056	3.4420	0.0409	-0.4271	3.3019

6.3.1. Damage detection using the proposed sensitivity method

Figs. 8 and 9 show the computed damage indices for both models of the composite plate when the SUIHP with NOM=4 and CFRF matrices are used for damage detection considering $NP = 30$. To asses the reliability of the proposed method against the measurement noise, 50 sets of the noisy CFRF data were considered. The developed computer program was set to solve the problem for each case after 100 iterations. The coefficient of variation (COV) was used in this paper to evaluate the performance of the algorithm when each of the CFRF and SUIHP is used for damage detection. The COV is defined as the normalized standard deviation of each damage index divided by its mean value [18]. As such, a smaller value of the COV corresponds to a more robust prediction of the damage indices.

Figs. 10 and 11 show the obtained values of the COV for different models of the composite plate using the SUIHP and CFRF matrices (NP=30). It is evident from the results that using SUIHP is more reliable than the CFRF.

6.4. Studying plates with different E_1/E_2 ratios

Thus far, the sensitivity of the proposed method to different values of the parameters of the studied plate including the number of ply and the orientation of the ply has been studied. In this section, the sensitivity of the proposed method to different values of E_1/E_2 ratio is considered. As such, this ratio was considered 20 and 30 here which is smaller than 40–the value considered in the previous sections. Table 7 lists the obtained natural frequencies of the laminated composite models for different values of the E_1/E_2 ratio. It can be noted that the natural frequencies of the composite plates were obtained smaller when this ratio was set at a smaller value. It can be also noted that the closely-situated eigenvelues issue still remains in the models. Next, the accuracy indices obtained for the performance of the proposed method applied to the composite laminate

Table 7: First ten natural frequencies of the simulated composite plates with different values of the E_1/E_2.

Lamination scheme		Mode No. 1	2	3	4	5	6	7	8	9	10
Intact, $E_1/E_2 = 20$	NoL = 3, LA = $(0°/90°/0°)$	6.74	10.13	13.60	15.33	17.52	20.34	22.64	23.14	25.46	25.72
	NoL = 6, LA = $(0°/45°/0°)$	6.89	10.59	13.87	15.85	18.06	20.95	21.14	22.96	23.98	25.76
Intact, $E_1/E_2 = 30$	NoL = 3, LA = $(0°/90°/0°)$	7.14	10.70	14.04	15.85	18.21	20.96	23.07	23.60	25.73	25.94
	NoL = 6, LA = $(0°/45°/0°)$	7.34	11.14	14.40	16.41	18.64	21.56	23.48	24.04	24.55	25.77
Case 1, $E_1/E_2 = 20$	NoL = 3, LA = $(0°/90°/0°)$	6.64	10.03	13.40	15.03	17.41	20.02	22.38	22.81	25.08	25.38
	NoL = 6, LA = $(0°/45°/0°)$	6.81	10.50	13.68	15.54	18.00	20.53	20.95	22.70	23.75	25.43
Case 1, $E_1/E_2 = 30$	NoL = 3, LA = $(0°/90°/0°)$	7.04	10.58	13.83	15.55	18.09	20.63	22.82	23.27	25.37	25.59
	NoL = 6, LA = $(0°/45°/0°)$	7.26	11.06	14.21	16.09	18.59	21.11	23.23	23.85	24.32	25.44

Table 8: The accuracy indicators obtained for the simulated composite plates with different values of the E_1/E_2.

Case	$\boldsymbol{E_1/E_2}$	**NP**	**NoL = 3, LA = 0°/90°/0°**			**NoL = 6, LA = 0°/45°/0°**		
No.		**(%)**	**MSE**	**RE**	**CI**	**MSE**	**RE**	**CI**
1	40	30	0.0024	-0.0931	0.9545	0.0037	-0.1158	0.9275
1	30	30	0.0026	-0.1001	0.9449	0.0040	-0.1172	0.9333
1	20	30	0.0027	-0.1112	0.9401	0.0041	-0.1177	0.9411

plates with different values of E_1/E_2 were evaluated. The results are presented in Table 8. The obtained accuracy results indicate the perfect performance of the proposed method considering different values of the E_1/E_2 ratio in the laminated composite plates.

6.5. Comparison with other methods

The proposed method of this paper is compared against two other methods in the literature through comparing the accuracy indices obtained for each method. Table 9 shows the accuracy indices obtained from the proposed method and the methods proposed in [12] and [20] in all damage scenarios. As such, the obtained values of the accuracy indices of MSE, RE, and CI clearly demonstrate the superiority of the proposed method when $NP = 30$.

7. Conclusions

In this study, a sensitivity-based damage detection method was proposed that uses the SUIHP corresponding to the measured/simulated CFRF signals as input. The results indicate that more accurate results can be achieved when SUIHP is used as opposed to the CFRF at the presence of high percentage of noise. Moreover, it was shown that the proposed feature is far more sensitive to damage compared with the case when CFRF is used as input. The proposed method was also compared against two other methods proposed in the literature. The results demonstrate the superiority of the proposed method in all cases of the simulated damage scenarios.

This paper presents several novelties including the proposed sensitivity-based damage detection method. However, the main novelty of this paper comes from the proposed SUIHP as

Table 9: Comparison of the accuracy indicators obtained for [12] and [20] with the proposed method.

Case	**Applied**	**NP**	**NoL = 3, LA = 0°/90°/0°**			**NoL = 6, LA = 0°/45°/0°**		
No.	**method**	**(%)**	**MSE**	**RE**	**CI**	**MSE**	**RE**	**CI**
1	Proposed	30	0.0024	-0.0931	0.9545	0.0037	-0.1158	0.9275
2	Proposed	30	0.0040	-0.1321	0.9349	0.0036	-0.1145	0.9423
3	Proposed	30	0.0044	-0.1312	0.9101	0.0046	-0.1377	0.9111
4	Proposed	30	0.0039	-0.1154	0.9306	0.0037	-0.0981	0.9394
5	Proposed	30	0.0043	-0.1364	0.9201	0.0059	-0.1639	0.8934
6	Proposed	30	0.0040	-0.1104	0.9399	0.0059	-0.1356	0.9130
1	[20]	30	0.3850	-0.9325	4.3658	0.4028	-0.7258	3.9985
2	[20]	30	0.4258	-0.9412	5.1002	0.3952	-0.8888	5.0023
3	[20]	30	0.3940	-0.9961	5.1036	0.4107	-0.6085	5.4411
4	[20]	30	0.5126	-0.8941	4.1478	0.3014	-0.7518	5.2478
5	[20]	30	0.5526	-0.7103	6.1000	0.4274	-0.6912	5.4020
6	[20]	30	0.5325	-0.7720	5.2369	0.3369	-0.7199	5.2236
1	[12]	30	0.4421	-0.9981	7.0023	0.5745	-0.9258	7.4102
2	[12]	30	0.4600	-0.9888	7.5002	0.4826	-0.9625	6.6273
3	[12]	30	0.4810	-0.9741	7.8246	0.6674	-0.9475	8.8852
4	[12]	30	0.4852	-0.9958	8.5478	0.5826	-0.9371	7.3270
5	[12]	30	0.5523	-0.9849	9.4250	0.6025	-0.9963	8.8963
6	[12]	30	0.5023	-0.9963	9.3975	0.6021	-0.9635	8.8230

a damage sensitive feature. As such, future work can be dedicated to testing the proposed technique in some other optimisation problems that use a set of signals as input. Based on the obtained results of this paper, the SUIHP of the identified signals is recommended to be used, instead of the signals themselves, as input to the objective function of the optimisation problem, especially when the identified signals are highly contaminated by measurement noise.

Although the proposed method was preliminary developed to address the damage detection problem in composite structures, further investigation of the applicability of the proposed method to composite materials can be a subject of future work. Moreover, the studied numerical examples of this paper were developed based on the assumption of fully clamped boundary conditions. However, care must be taken when it comes to conduct damage detection in a real composite structure, where a more realistic assumption for the rigidity of its supports needs to be made in the constructed FE model. Finally, the present study, in its current form, aims to propose a novel concept through coupling an advanced signal processing method with the classical concept of FRFs for overcoming the challenge of using highly noisy measurements for damage detection in laminated composite plates, as examples of structures with closely-situated eigenvalues. The authors are keen to validate the results of this paper through an experimental study in their future work.

References

[1] Barman SK, Maiti DK, Maity D. Vibration-based delamination detection in composite structures employing mixed unified particle swarm optimization. AIAA Journal 2021;59(1):386–99. doi:10.2514/1.J059176.

[2] Guo F, Wu JH. Analytical solution and coupling resonance mechanism of interface delamination of composite laminates excited by ultrasonic shear horizontal waves. Composite Structures 2021;:114583doi:10.1016/j.compstruct.2021.114583.

[3] Köllner A. Predicting buckling-driven delamination propagation in composite laminates: An analytical modelling approach. Composite Structures 2021;266:113776. doi:10.1016/j.compstruct.2021.113776.

[4] Khan A, Khalid S, Raouf I, Sohn JW, Kim HS. Autonomous assessment of delamination using scarce raw structural vibration and transfer learning. Sensors 2021;21(18):6239. doi:https://doi.org/10.3390/s21186239.

[5] Khan A, Ko DK, Lim SC, Kim HS. Structural vibration-based classification and prediction of delamination in smart composite laminates using deep learning neural network. Composites Part B: Engineering 2019;161:586–94. doi:https://doi.org/10.1016/j.compositesb.2018.12.118.

[6] Khan A, Kim HS. Assessment of delaminated smart composite laminates via system identification and supervised learning. Composite Structures 2018;206:354–62. doi:https://doi.org/10.1016/j.compstruct.2018.08.014.

[7] Güemes A, Fernandez-Lopez A, Pozo AR, Sierra-Pérez J. Structural health monitoring for advanced composite structures: a review. Journal of Composites Science 2020;4(1):13. doi:10.3390/jcs4010013.

[8] Khatir S, Wahab MA. A computational approach for crack identification in plate structures using xfem, xiga, pso and jaya algorithm. Theoretical and Applied Fracture Mechanics 2019;103:102240. doi:10.1016/j.tafmec.2019.102240.

[9] Hou R, Xia Y. Review on the new development of vibration-based damage identification for civil engineering structures: 2010–2019. Journal of Sound and Vibration 2020;:115741doi:10.1016/j.jsv.2020.115741.

[10] Dos Santos JA, Soares CM, Soares CM, Maia N. Structural damage identification in laminated structures using frf data. Composite Structures 2005;67(2):239–49. doi:10.1016/j.compstruct.2004.09.011.

[11] Icardi U, Ferrero L. Impact analysis of sandwich composites based on a refined plate element with strain energy updating. Composite Structures 2009;89(1):35–51. doi:10.1016/j.compstruct.2008.06.018.

[12] Vo-Duy T, Ho-Huu V, Dang-Trung H, Nguyen-Thoi T. A two-step approach for damage detection in laminated composite structures using modal strain energy method and an improved differential evolution algorithm. Composite Structures 2016;147:42–53. doi:10.1016/j.compstruct.2016.03.027.

[13] Xie H, Fang H, Li X, Wan L, Wu P, Yu Y. Low-velocity impact damage detection and characterization in composite sandwich panels using infrared thermography. Composite Structures 2021;269:114008. doi:10.1016/j.compstruct.2021.114008.

[14] Tarfaoui M, El Moumen A, Yahia HB. Damage detection versus heat dissipation in e-glass/epoxy laminated composites under dynamic compression at high strain rate. Composite Structures 2018;186:50–61. doi:10.1016/j.compstruct.2017.11.083.

[15] Pedram M, Esfandiari A, Khedmati MR. Finite element model updating using strain-based power spectral density for damage detection. Structural Control and Health Monitoring 2016;23(11):1314–33. doi:10.1002/stc.1833.

[16] Esfandiari A, Nabiyan MS, Rofooei FR. Structural damage detection using principal component analysis of frequency response function data. Structural Control and Health Monitoring 2020;27(7):e2550. doi:10.1002/stc.2550.

[17] Friswell M, Mottershead JE. Finite element model updating in structural dynamics; vol. 38. Springer Science & Business Media; 2013.

[18] Shadan F, Khoshnoudian F, Esfandiari A. A frequency response-based structural damage identification using model updating method. Structural Control and Health Monitoring 2016;23(2):286–302. doi:10.1002/stc.1768.

[19] Esfandiari A, Bakhtiari-Nejad F, Rahai A, Sanayei M. Structural model updating using frequency response function and quasi-linear sensitivity equation. Journal of sound and vibration 2009;326(3-5):557–73. doi:10.1016/j.jsv.2009.07.001.

[20] Fallah N, Vaez SRH, Fasihi H. Damage identification in laminated composite plates using a new multi-step approach. Steel and Composite Structures 2018;29(1):139–49. doi:10.12989/scs.2018.29.1.139.

[21] Dinh-Cong D, Nguyen-Thoi T, Nguyen DT. A two-stage multi-damage detection approach for composite structures using mkecr-tikhonov regularization iterative method and model updating procedure. Applied Mathematical Modelling 2021;90:114–30. doi:10.1016/j.apm.2020.09.002.

[22] Liu X, Hu J. On the placement of actuators and sensors for flexible structures with closely spaced modes. Science China Technological Sciences 2010;53(7):1973–82. doi:10.1007/s11431-010-4028-y.

[23] Arora V, Singh S, Kundra T. Damped model updating using complex updating parameters. Journal of Sound and Vibration 2009;320(1-2):438–51. doi:10.1016/j.jsv.2008.08.014.

[24] Chen S, Ong ZC, Lam WH, Lim KS, Lai KW. Operational damage identification scheme utilizing de-noised frequency response functions and artificial neural network. Journal of Nondestructive Evaluation 2020;39(3):1–9. doi:doi.org/10.1007/s10921-020-00709-x.

[25] Feng D, Feng MQ. Computer vision for shm of civil infrastructure: From dynamic response measurement to damage detection–a review. Engineering Structures 2018;156:105–17. doi:10.1016/j.engstruct.2017.11.018.

[26] Mousavi M, Holloway D, Olivier J. A new signal reconstruction for damage detection on a simply supported beam subjected to a moving mass. Journal of Civil Structural Health Monitoring 2020;10(4):709–28. doi:10.1007/s13349-020-00414-3.

[27] Ganguli R. Wavelet based damage detection. In: Structural health monitoring. Springer; 2020, p. 161–92.

[28] Ma Q, Solís M, Galvín P. Wavelet analysis of static deflections for multiple damage identification in beams. Mechanical Systems and Signal Processing 2021;147:107103. doi:10.1016/j.ymssp.2020.107103.

[29] Mousavi M, Taskhiri MS, Holloway D, Olivier J, Turner P. Feature extraction of wood-hole defects using empirical mode decomposition of ultrasonic signals. NDT & E International 2020;114:102282. doi:10.1016/j.ndteint.2020.102282.

[30] Wang L, Shao Y. Fault feature extraction of rotating machinery using a reweighted complete ensemble empirical mode decomposition with adaptive noise and demodulation analysis. Mechanical Systems and Signal Processing 2020;138:106545. doi:10.1016/j.ymssp.2019.106545.

[31] Mousavi M, Holloway D, Olivier J, Gandomi AH. Beam damage detection using synchronisation of peaks in instantaneous frequency and amplitude of vibration data. Measurement 2021;168:108297.

[32] Dragomiretskiy K, Zosso D. Variational mode decomposition. IEEE Transactions on Signal Processing 2014;62(3):531–44. doi:10.1109/TSP.2013.2288675.

[33] Mousavi M, Gandomi AH. An input-output damage detection method using static equivalent formulation of dynamic vibration. Archives of Civil and Mechanical Engineering 2018;18:508–14. doi:10.1016/j.acme.2017.01.007.

[34] Muskhelishvili Nikolaĭ I, Radok JRM. Singular integral equations: boundary problems of function theory and their application to mathematical physics. Courier Corporation; 2008.

[35] Hildebrand FB. Advanced calculus for engineers. Prentice-Hall; 1949.

[36] Gabor D. Theory of communication. part 1: The analysis of information. Journal of the Institution of Electrical Engineers-Part III: Radio and Communication Engineering 1946;93(26):429–41.

[37] Boller C, Chang FK, Fujino Y. Encyclopedia of structural health monitoring. Wiley; 2009.

[38] Zosso D. Variational mode decomposition, matlab central file exchange. Retrieved August 27, 2020. URL: https://www.mathworks.com/matlabcentral/fileexchange/44765-variational-mode-decomposition.

[39] Wang Y, Markert R, Xiang J, Zheng W. Research on variational mode decomposition and its application in detecting rub-impact fault of the rotor system. Mechanical Systems and Signal Processing 2015;60:243–51. doi:https://doi.org/10.1016/j.ymssp.2015.02.020.

[40] Mousavi M, Gandomi AH. Wood hole-damage detection and classification via contact ultrasonic testing. Construction and Building Materials 2021;307:124999. doi:https://doi.org/10.1016/j.conbuildmat.2021.124999.

[41] Mousavi M, Gandomi AH. Prediction error of johansen cointegration residuals for structural health monitoring. Mechanical Systems and Signal Processing 2021;160:107847. doi:https://doi.org/10.1016/j.ymssp.2021.107847.

[42] Mousavi M, Gandomi AH. Structural health monitoring under environmental and operational variations using mcd prediction error. Journal of Sound and Vibration 2021;512:116370. doi:https://doi.org/10.1016/j.jsv.2021.116370.

[43] Mousavi M, Gandomi AH. Deep learning for structural health monitoring under environmental and operational variations. In: Nondestructive Characterization and Monitoring of Advanced Materials, Aerospace, Civil Infrastructure, and Transportation XV; vol. 11592. International Society for Optics and Photonics; 2021, p. 115920H. doi:https://doi.org/10.1117/12.2582649.

[44] Hassani S, Shadan F. Using incomplete frf measurements for damage detection of structures with closely-spaced eigenvalues. Measurement 2021;:110388doi:https://doi.org/10.1016/j.measurement.2021.110388.

[45] Pereira J, Heylen W, Lammens S, Sas P. Influence of the number of frequency points and resonance frequencies on modal updating techniques for health condition monitoring and damage detection of flexible structure. In: Proceedings-SPIE The International Society for Optical Engineering. Citeseer; 1995, p. 1273–.

[46] Reddy JN. Mechanics of laminated composite plates and shells: theory and analysis. CRC press; 2003.

[47] Ferreira A, Castro LM, Bertoluzza S. A high order collocation method for the static and vibration analysis of composite plates using a first-order theory. Composite structures 2009;89(3):424–32. doi:10.1016/j.compstruct.2008.09.006.

[48] Ferreira A, Fasshauer G. Computation of natural frequencies of shear deformable beams and plates by an rbf-pseudospectral method. Computer Methods in Applied Mechanics and Engineering 2006;196(1-3):134–46. doi:10.1016/j.cma.2006.02.009.

[49] Ferreira A, Fasshauer G. Analysis of natural frequencies of composite plates by an rbf-pseudospectral method. Composite structures 2007;79(2):202–10. doi:10.1016/j.compstruct.2005.12.004.

[50] Ferreira A, Roque C, Martins P. Analysis of composite plates using higher-order shear deformation theory and a finite point formulation based on the multiquadric radial basis function method. Composites Part B: Engineering 2003;34(7):627–36. doi:10.1016/S1359-8368(03)00083-0.

[51] Brincker R, Lopez-Aenlle M. Mode shape sensitivity of two closely spaced eigenvalues. Journal of Sound and Vibration 2015;334:377–87. doi:10.1016/j.jsv.2014.08.015.

[52] Nelson RB. Simplified calculation of eigenvector derivatives. AIAA journal 1976;14(9):1201–5. doi:10.2514/3.7211.

[53] Au SK, Brownjohn JM, Li B, Raby A. Understanding and managing identification uncertainty of close modes in operational modal analysis. Mechanical Systems and Signal Processing 2021;147:107018. doi:10.1016/j.ymssp.2020.107018.

[54] He WY, Ren WX, Zhu S. Damage detection of beam structures using quasi-static moving load induced displacement response. Engineering Structures 2017;145:70–82. doi:10.1016/j.engstruct.2017.05.009.

[55] Al-Hazmi MW. Finite element analysis of cantilever plate structure excited by patches of piezoelectric actuaturs. In: 2008 11th Intersociety Conference on Thermal and Thermomechanical Phenomena in Electronic Systems. IEEE; 2008, p. 809–14. doi:10.1109/ITHERM.2008.4544350.

[56] Aliabadi MF, Khodaei ZS. Structural health monitoring for advanced composite structures; vol. 8. World Scientific; 2017.